Electronic Supplementary Material (ESI) for Energy & Environmental Science.
This journal is © The Royal Society of Chemistry 2016

Oxygen electroreduction catalysed by laccase wired to gold nano-particles *via* the trinuclear copper cluster

Marius Dagys, Audrius Laurynėnas, Dalius Ratautas, Juozas Kulys, Regina Vidžiūnaitė, Martynas Talaikis, Gediminas Niaura, Liucija Marcinkevičienė, Rolandas Meškys and Sergey Shleev

SUPPORTING INFORMATION

Materials and Methods

Chemicals. Gold (III) chloride trihydrate, 2,2′-azinobis-(3-ethylbenzothiazoline-6-sulfonic acid) ammonium salt (ABTS), potassium ferrocyanide ($K_4[Fe(CN)_6]$), 4-mercaptobenzoic acid, sodium fluoride, sodium citrate, sodium sulphate, ammonium sulphate, potassium dihydrogen phosphate, hydrogen peroxide, sulfuric and citric acids were purchased from Sigma-Aldrich (St Louis, MO, USA). Sodium hydrogen phosphate and disodium hydrogen phosphate were purchased from Carl Roth GmbH (Karlsruhe, Germany). Bovine serum albumin (BSA) was from Serva GmbH (Heidelberg, Germany). All reagents were of analytical grade, and all solutions were prepared using deionized water (18.2 MΩ cm).

Enzyme. Laccase from *Didymocrea* sp.J6 (LAC) was purified according to the procedure described previously.[1] The fungus *Didymocrea* sp. J6 was cultivated in flasks with 200 ml of media consisting of: malt extract – 3.5 g L^{-1}, yeast extract – 2.5 g L^{-1}, $MgSO_4$ – 0.5 g L^{-1}, glucose – 0.8 g L^{-1}, KH_2PO_4 – 1.0 g L^{-1}, and $CuSO_4$ – 0.2 mM, pH 6.5. The culture was grown aerobically at 30 °C for 3 days. The mycelium was removed by filtration, and sorbent DEAE Toyopearl 650M from Tosoh Corporation (Tokyo, Japan), equilibrated with 5 mM potassium phosphate buffer pH 7.0, was added to the culture liquid (15 mL of sorbent to 1 L of cultural liquid) containing extracellular LAC. The mixture was stirred for 2 h at room temperature. After sedimentation the sorbent was washed with 5 mM potassium phosphate buffer, pH 7.0, and loaded into a column, and the LAC was eluted using a linear gradient of 5 to 500 mM of potassium phosphate buffer, pH 7.0. Fractions displaying enzymatic activity were collected, concentrated, supplemented with 1 M ammonium sulphate, and applied onto a Source 15PHE column (10 mm ID x 10 cm) from GE Healthcare (Uppsala, Sweden), equilibrated with potassium phosphate buffer, pH 7.0, 1 M ammonium sulphate. LAC was eluted using a linear gradient of 1.0–0 M of ammonium sulphate in the same buffer solution. Active fractions were concentrated, dialyzed overnight against 5 mM potassium phosphate buffer, pH 7.0, and applied onto a Source 15Q column (5 mm ID x 20 cm, GE Healthcare,

Sweden). The enzyme was eluted using a linear gradient of 0–0.5 M of potassium phosphate buffer, pH 7.0. Fraction displaying LAC activity were concentrated and stored at –20 °C.

The enzyme was found to be homogeneous with a single band on 14% SDS-PAGE with a molecular mass of 49 kDa. Protein concentration was measured routinely by the Lowry method[2] using BSA as a standard. The activity of LAC was routinely assayed by monitoring the oxidation of ABTS to its radical cation ($ABTS^{+\cdot}$) spectrophotometrically at 420 nm (ε_{420} = 36 000 M^{-1} cm^{-1}). The reaction mixture contained 0.25 mM ABTS (50 mM sodium citrate buffer, pH 3.5) and a suitable amount of the enzyme. One unit of activity was defined as the amount of LAC catalysing the formation of 1 μmol of $ABTS^{+\cdot}$ per minute at 30 °C. After purification, the fractions displaying activity were collected, concentrated and dialyzed against 5 mM potassium phosphate buffer, pH 7.0 and stored at –20 °C. Before an experiment, the enzyme was diluted to the required concentration and kept at 4–8°C for 1–2 days only.

Enzyme glycosylation. The amount of glycosides in the protein molecule was established in order to provide background information of relevance for understanding the efficient DET-based bioelectrocatalysis of AuNP-LAC conjugate (*vide infra*). In brief, 20 μg of LAC was incubated without denaturation in 100 mM sodium citrate buffer solution, pH 5.5 containing 2.5 mU of Endoglycosidase H from *Streptomyces*, purchased from Sigma-Aldrich (St Louis, MO, USA), for 20 h at 37 °C. Molecular masses of treated and untreated LAC were determined by 10% SDS-PAGE. Observation of differences in molecular masses of Endoglycosidase-H treated and untreated enzyme batches showed that glycosylation of LAC from *Didymocrea* sp. J6 is negligible and carbohydrate content does not exceed a few percent of the total mass of the enzyme. The efficiency of the method used was confirmed by running the same experiment using another batch of LAC with known glycosylation level.

Kinetic measurements in homogeneous solutions. Homogeneous kinetic experiments were carried out using a thermostated quartz cuvette (optical path length – 1 cm) at 25 °C with ThermoScientific™ Evolution™ 300 UV-Vis spectrophotometer from Thermo Scientific (Waltham, MA, USA). Buffer solu-

tions were thermostated before the experiments to ensure the same oxygen concentration in all measurements. Oxidation of ABTS and ferrocyanide was monitored at 420 nm, where absorbance increases are due to formation of $ABTS^{+\cdot}$ (ε_{420}= 36 mM^{-1} cm^{-1}) or ferricyanide (ε_{420}= 1 mM^{-1} cm^{-1}). The initial concentration of ABTS and ferrocyanide in these studies was varied from 3.75 to 30 μM and from 22 to 200 μM, respectively. Initial oxygen concentration was assumed to be 253 μM. Initial concentrations of the enzyme during experiments at pH 4.0, 5.5 and 7.4 were 8.0, 8.0, and 55 nM, respectively. The catalytic reaction scheme of LAC used in data analysis of the experimental results was based on the mechanism of MCO function previously developed by Solomon and co-workers:[3]

$$Lac_{resting} + S_{red} \xrightarrow{k_{act}} Lac_2 + S_{ox} \quad \text{(Supporting Eq. S1)}$$

$$Lac_1 + S_{red} \xrightarrow{k_{red}} Lac_2 + S_{ox} \quad \text{(Supporting Eq. S2)}$$

$$Lac_2 + S_{red} \xrightarrow{k_{red}} Lac_3 + S_{ox} \quad \text{(Supporting Eq. S3)}$$

$$Lac_3 + S_{red} \xrightarrow{k_{red}} Lac_4 + S_{ox} \quad \text{(Supporting Eq. S4)}$$

$$Lac_4 + S_{red} \xrightarrow{k_{red}} Lac_{red} + S_{ox} \quad \text{(Supporting Eq. S5)}$$

$$Lac_{red} + O_2 \xrightarrow{k_{ox}} Lac_1 + 2H_2O \quad \text{(Supporting Eq. S6)}$$

$$Lac_1 \xrightarrow{k_{inact}} Lac_{resting} \quad \text{(Supporting Eq. S7)}$$

$$Lac_1 + F^- \underset{k_b}{\overset{k_f}{\rightleftarrows}} LacF \quad \text{(Supporting Eq. S8)}$$

$$k_{red} = \frac{k_1 k_2 k_3 k_4}{k_1 k_2 k_3 + k_1 k_2 k_4 + k_1 k_3 k_4 + k_2 k_3 k_4} \quad \text{(Supporting Eq. S9)}$$

$$K_{inh} = \frac{k_b}{k_f} \quad \text{(Supporting Eq. S10)}$$

Here S_{red} and S_{ox} are reduced and oxidized forms of the substrate (ABTS or ferrocyanide); $Lac_{resting}$ – resting form of the enzyme; Lac_1, Lac_2, Lac_3 and Lac_4 – enzyme forms at four different stages of one-electron reduction of LAC; Lac_{red} – fully reduced enzyme form; k_{act} – apparent bimolecular enzyme activation rate constant, k_1, k_2, k_3 and k_4 – apparent bimolecular one-electron reduction constants; k_{red} –

reduction of k_1, k_2, k_3 and k_4 into a limiting step apparent rate constant as expressed in Eq. S9; k_{ox} – apparent bimolecular enzyme oxidation rate constant; k_{inact} – LAC inactivation rate constant; k_f and k_b – association and dissociation rate constants of fluoride interacting with the LAC active centre, respectively; K_{inh} – enzyme inhibition constant. All the rate parameters were fitted to the experimental kinetic curves using rModeler software from Ubique Calculus Ltd. (Vilnius, Lithuania).[4]

Electrochemical Measurements. Electrochemical experiments were performed with a Series G™ 750 Potentiostat/Galvanostat/ZRA from Gamry Instruments, Inc. (Warminster, PA, USA), controlled by dedicated PHE200™ software. All experiments were carried out in a three-electrode glass cell using an Ag|AgCl|3M KCl reference electrode (210 mV *vs.* NHE) and a platinum wire counter electrode from BASi (West Lafayette, IN, USA). Rotating gold disc electrodes were utilized in conjunction with a RDE-2 rotating disc electrode system also from BASi. All electrochemical measurements were performed in a working buffer solution (WBS) containing 50 mM disodium phosphate and 100 mM sodium sulphate; pH was adjusted by addition of citric acid. Solutions containing sodium fluoride had their pH adjusted after addition of fluoride.

Electrode preparation. AuNPs were obtained by the citrate reduction procedure.[5,6] The size and concentration of the synthesized AuNPs were determined spectrophotometrically[7] and found to be 30 ± 5 nm. To concentrate AuNPs, the solution was centrifuged at 10000 rpm for 10 min and 95 % of the supernatant was removed. A rotating disk polycrystalline gold electrode (diameter – 3 mm) was polished using alumina paste (0.3 μm diameter from Buehler (Lake Bluff, IL, USA)), ultra-sonicated for 10 min, rinsed with water, and cleaned by 30 electrochemical oxidation-reduction cycles in 0.5 M sulfuric acid between 0 and 1.9 V *vs.* NHE at a scan rate of 0.3 V s^{-1} to eliminate traces of citrate.[8] Afterwards, 5 μL of concentrated AuNP solution was pipetted onto the electrode surface and allowed to dry, and then the electrode was cleaned again by 40 cycles of electrochemical oxidation-reduction and thoroughly rinsed with water.

Enzyme immobilization. LAC was electrostatically adsorbed on AuNP-covered electrode surfaces by immersing modified electrodes into an enzyme-containing solution, *viz.* 2.79 μg mL^{-1} (57.0 nM) LAC dissolved in a buffer solution containing 50 mM sodium phosphate, 100 mM sodium sulphate, and pH 5.5 adjusted by citric acid. Part of the solution was saved as a control for later measurements. After immersion of the electrode a fixed potential (between 200 and 1000 mV *vs.* NHE, *vide supra*) was applied for 30 min at room temperature. After removal of electrodes from the electrolyte the total activity of the remaining enzyme in solution was measured spectrophotometrically using 5 mM ABTS as substrate and compared to the initial value in the control solution. The concentration of LAC in solution was chosen by consideration that the observed activity drop should be 5 % or higher in order to reliably estimate the amount of enzyme adsorbed on the electrode surface. This electrode is further referred to as AuNP/LAC.

For measurements when the goal was to produce an enzyme facing AuNP surface by T1 Cu site, another enzyme immobilization technique was used. AuNP-covered electrodes were immersed into argon saturated methanol solution containing 2 mM 4-mercaptobenzoic acid (4-MBA) for 24 hours, then rinsed with argon saturated methanol and de-ionised water, respectively. Afterwards, 5 μL of solution containing LAC (3.10 mg mL^{-1}) was dispensed on the electrode surface and kept for 2 hours under humid conditions to avoid evaporation. Before measurements the electrodes were thoroughly rinsed by solution containing 50 mM sodium phosphate, 100 mM sodium sulphate, and pH 4.0 adjusted by citric acid. This electrode is further referred to as AuNP/MBA/LAC.

Modelling of heterogeneous LAC-AuNP systems. Derivation of the mathematical description of the catalytic scheme presented in ***Figure 1B***, featuring direct electron transfer from the electrode surface to the **T2/T3 Cu cluster**, required establishment of the following assumptions:

- Electrochemical measurements were made in oxygen concentrations lower than the Michaelis constant (as was confirmed by K_M calculations, *cf.* Figure S1 A).

- The impact of the T1 Cu site in heterogeneous ET is negligible and ET occurs only between the T2/T3 Cu cluster and AuNP surface.
- Fluoride ions bind to the T2/T3 Cu cluster and affect both the heterogeneous ET rate and the apparent bimolecular oxygen reduction rate constants.
- Fluoride-ion inhibition constants are the same for reduced and oxidized forms of the T2/T3 Cu cluster.
- Bioelectrocatalytic current is limited by the catalytic oxygen reduction by LAC and/or heterogeneous ET, not by oxygen diffusion towards the electrode surface.
- The enzyme – fluoride association constant value approaches the diffusion limit.
- Electron transfer between electrode and T2/T3 cluster can be described by one-electron limiting step.

To describe the process a system of differential equations was constructed:

$$\frac{d\Gamma^{O}}{dt} = k_2\Gamma^{R} - k_1\Gamma^{O} + k_{ox}\Gamma^{R}[\mathrm{O_2}] + k_d^f\Gamma^{FO} - k_a^f\Gamma^{O}[\mathrm{F^-}] \qquad \text{(Supporting Eq. S11)}$$

$$\frac{d\Gamma^{R}}{dt} = k_1\Gamma^{O} - k_{-1}\Gamma^{R} + k_{ox}\Gamma^{R}[\mathrm{O_2}] + k_d^f\Gamma^{FR} - k_a^f\Gamma^{R}[\mathrm{F^-}] \qquad \text{(Supporting Eq. S12)}$$

$$\frac{d\Gamma^{FO}}{dt} = k_{-1}^f\Gamma^{FR} - k_1^f\Gamma^{FO} + k_{ox}\Gamma^{FR}[\mathrm{O_2}] + k_a^f\Gamma^{O}[\mathrm{F^-}] - k_d^f\Gamma^{FO} \qquad \text{(Supporting Eq. S13)}$$

$$\frac{d\Gamma^{FR}}{dt} = -k_{-1}^f\Gamma^{FR} + k_1^f\Gamma^{FO} - k_{ox}^f\Gamma^{FR}[\mathrm{O_2}] - k_d^f\Gamma^{FR} + k_a^f\Gamma^{R}[\mathrm{F^-}] \qquad \text{(Supporting Eq. S14)}$$

Here Γ (mol cm^{-2}) represents surface coverage by various oxidation and fluoride binding states of LAC, and [F^-] and [O_2] are bulk concentrations (mol cm^{-3}) of fluoride ions and oxygen, respectively. Assuming steady state and adding the mass balance equation for Γ:

$$\Gamma^{O} + \Gamma^{R} + \Gamma^{FO} + \Gamma^{FR} = \Gamma^{Tot} \qquad \text{(Supporting Eq. S15)}$$

together with the current density equation:

$$j = \frac{i}{A} = -nF(k_{ox}^{f}\Gamma^{FR}[O_2] + k_{ox}\Gamma^{R}[O_2]) \quad \text{(Supporting Eq. S16)}$$

it is possible to solve for all surface coverages of enzyme forms and put the solutions into the current density equation, substitute the fluoride dissociation rate constants with $k_d^f \rightarrow k_a^f K_{inh}$, and simplify the expression by choosing the limit $k_a^f \rightarrow \infty$. The resulting equation for current density becomes:

$$j = \frac{-nF\Gamma^{Tot}[\mathrm{O_2}]([\mathrm{F^-}]k_1^f + k_1 K_{inh})([\mathrm{F^-}]k_{ox}^f + K_{inh}k_{ox})}{([\mathrm{F^-}] + K_{inh})([\mathrm{F^-}]\left(k_1^f + k_{-1}^f + k_{ox}^f[\mathrm{O_2}]\right) + K_{inh}(k_1 + k_{-1} + k_{ox}[\mathrm{O_2}]))} \quad \text{(Supporting Eq. S17)}$$

where:

$$k_1 = k_0 e^{-\alpha(E - E^0_{T2/T3})\frac{F}{RT}} \quad \text{(Supporting Eq. S18)}$$

$$k_{-1} = k_0 e^{(1-\alpha)(E - E^0_{T2/T3})\frac{F}{RT}} \quad \text{(Supporting Eq. S19)}$$

$$k_1^f = k_0^f e^{-\alpha^f(E - E^0_{T2/T3-F})\frac{F}{RT}} \quad \text{(Supporting Eq. S20)}$$

$$k_{-1}^f = k_0^f e^{(1-\alpha^f)(E - E^0_{T2/T3-F})\frac{F}{RT}} \quad \text{(Supporting Eq. S21)}$$

$$\frac{k_d^f}{k_a^f} = K_{inh} \quad \text{(Supporting Eq. S22)}$$

Here k_0 and k_0^F are heterogeneous ET rate constant of native and inhibited enzyme, respectively; α and α^F are charge transfer coefficients from Butler–Volmer formulation for native and inhibited enzyme, respectively; $E^0_{T2/T3}$ and $E^0_{T2/T3-F}$ are redox potentials of native and fluoride-inhibited T2/T3 Cu site, respectively; and k_{ox} and k_{ox}^F – bimolecular oxidation constants for native and inhibited enzyme, respectively. This mathematical description was applied to cathodic-side scans of CVs presented in the left panel of Figure 2, with background currents removed; modelling results are presented in Table S4.

Surface plots generated by using the calculated results, Eq. S15-22, plotted over experimental data, are presented in right panel of Figure 2. Modelling was performed employing Wolfram Mathematica 9 software from Wolfram Research (Champaign, IL, USA), all the biocathodic curves from measurements at the same pH but different NaF concentrations were included into a single global analysis model.

Derivation of the mathematical description of the alternative catalytic scheme presented in ***Figure 1A***, featuring direct electron transfer from the electrode surface first to **T1 Cu** then to the T2/T3 Cu cluster, required establishment of similar assumptions:

- Electrochemical measurements were made in oxygen concentrations lower than the Michaelis constant.
- Fluoride ions bind to the T2/T3 Cu cluster and affect both internal ET rate and apparent bimolecular oxygen reduction rate constants. Heterogeneous ET rate constant between the electrode and T1 is unaffected upon fluoride binding to the T2/T3 cluster.
- Fluoride-ion inhibition constants are the same for reduced and oxidized forms of the T2/T3 Cu cluster.
- Bioelectrocatalytic current is limited by catalytic oxygen reduction by LAC and/or heterogeneous ET, not by oxygen diffusion towards the electrode surface.
- The enzyme – fluoride association constant value approaches the diffusion limit.
- Electron transfer between the electrode and the T2/T3 cluster can be described by one-electron limiting step.

To describe the process a system of differential equations was constructed:

$$\frac{d\Gamma_{T2/T3\ O}^{T1\ O}}{dt} = -k_1\Gamma_{T2/T3\ O}^{T1\ O} + k_{-1}\Gamma_{T2/T3\ O}^{T1\ R} + k_{ox}\Gamma_{T2/T3\ R}^{T1\ O}[\mathrm{O_2}] - k_a^f\Gamma_{T2/T3\ O}^{T1\ O}[\mathrm{F^-}] + k_d^f\Gamma_{T2/T3\ OF}^{T1\ O}$$

(Supporting Eq. S23)

$$\frac{d\Gamma^{T1\,O}_{T2/T3\,OF}}{dt} = k_a^f \Gamma^{T1\,O}_{T2/T3\,O}[\mathrm{F^-}] - k_d^f \Gamma^{T1\,O}_{T2/T3\,OF} - k_1^f \Gamma^{T1\,O}_{T2/T3\,OF} + k_{-1}^f \Gamma^{T1\,R}_{T2/T3\,OF} + k_{ox}^f \Gamma^{T1\,O}_{T2/T3\,RF}[\mathrm{O_2}]$$

(Supporting Eq. S24)

$$\frac{d\Gamma^{T1\,O}_{T2/T3\,R}}{dt} = k_1 \Gamma^{T1\,R}_{T2/T3\,O} - k_{-1} \Gamma^{T1\,O}_{T2/T3\,R} - k_{ox} \Gamma^{T1\,O}_{T2/T3\,R}[\mathrm{O_2}] - k_a^f \Gamma^{T1\,O}_{T2/T3\,R}[\mathrm{F^-}] + k_d^f \Gamma^{T1\,O}_{T2/T3\,RF}$$

(Supporting Eq. S25)

$$\frac{d\Gamma^{T1\,O}_{T2/T3\,RF}}{dt} = k_a^f \Gamma^{T1\,O}_{T2/T3\,R}[\mathrm{F^-}] - k_d^f \Gamma^{T1\,O}_{T2/T3\,RF} + k_2^f \Gamma^{T1\,R}_{T2/T3\,OF} - k_{-2}^f \Gamma^{T1\,O}_{T2/T3\,RF} - k_{ox}^f \Gamma^{T1\,O}_{T2/T3\,RF}[\mathrm{O_2}]$$

(Supporting Eq. S26)

$$\frac{d\Gamma^{T1\,R}_{T2/T3\,O}}{dt} = k_1 \Gamma^{T1\,O}_{T2/T3\,R} - k_{-1} \Gamma^{T1\,R}_{T2/T3\,O} - k_2 \Gamma^{T1\,R}_{T2/T3\,O} + k_{-2}^f \Gamma^{T1\,O}_{T2/T3\,R} - k_a^f \Gamma^{T1\,R}_{T2/T3\,O}[\mathrm{F^-}] + k_d^f \Gamma^{T1\,R}_{T2/T3\,OF}$$

(Supporting Eq. S27)

$$\frac{d\Gamma^{T1\,R}_{T2/T3\,OF}}{dt} = k_a^f \Gamma^{T1\,R}_{T2/T3\,O}[\mathrm{F^-}] - k_d^f \Gamma^{T1\,R}_{T2/T3\,OF} + k_1^f \Gamma^{T1\,O}_{T2/T3\,OF} - k_{-1}^f \Gamma^{T1\,R}_{T2/T3\,OF} - k_2^f \Gamma^{T1\,R}_{T2/T3\,OF} - k_{-2}^f \Gamma^{T1\,O}_{T2/T3\,RF}$$

(Supporting Eq. S28)

Here Γ (mol cm^{-2}) are surface coverage by various oxidation and fluoride binding states of LAC T1 and T2/T3 Cu clusters (*e.g.* $\Gamma^{T1\,R}_{T2/T3\,O}$ denotes surface coverage of enzyme form with reduced T1 and oxidised T2/T3 Cu clusters, $\Gamma^{T1\,R}_{T2/T3\,OF}$ refers to enzyme form with reduced T1 and fluoride-containing oxidised T2/T3 Cu clusters), [F$^-$] and [O_2] are bulk concentrations (mol cm^{-3}) of fluoride ions and oxygen, respectively. Assuming steady state and adding a mass balance equation for Γ:

$$\Gamma^{T1\,O}_{T2/T3\,O} + \Gamma^{T1\,O}_{T2/T3\,OF} + \Gamma^{T1\,O}_{T2/T3\,R} + \Gamma^{T1\,O}_{T2/T3\,RF} + \Gamma^{T1\,R}_{T2/T3\,O} + \Gamma^{T1\,R}_{T2/T3\,OF} = \Gamma^{Tot} \qquad \text{(Supporting Eq. S29)}$$

together with the current density equation:

$$j = \frac{i}{A} = -nF(k_{ox}^f \Gamma^{FR}[O_2] + k_{ox} \Gamma^{R}[O_2]) \qquad \text{(Supporting Eq. S30)}$$

it is possible to solve for all surface coverages of enzyme forms and put solutions into the current density equation, substitute fluoride dissociation rate constants with $k_d^f \rightarrow k_a^f K_{inh}$, and simplify the expression by choosing the limit $k_a^f \rightarrow \infty$. The resulting equation for current density is:

$$j = \frac{-nF\Gamma^{Tot}[\mathrm{O_2}]\left([\mathrm{F^-}]k_1^f + K_{inh}k_1\right)\left([\mathrm{F^-}]k_2^f + K_{inh}k_2\right)\left([\mathrm{F^-}]k_{ox}^f + K_{inh}k_{ox}\right)}{([\mathrm{F^-}]+K_{inh})\Big[[\mathrm{F^-}]^2\left([\mathrm{O_2}]k_{ox}^f k_2^f + k_{-1}^f(k_{-2}^f + [\mathrm{O_2}]k_{ox}^f) + k_1^f\left(k_2^f + k_{-2}^f + k_{ox}^f\right)[\mathrm{O_2}]\right) + \\ + K_{inh}{}^2\left([\mathrm{O_2}]k_{ox}k_2 + k_{-1}([\mathrm{O_2}]k_{ox} + k_{-2}) + k_1([\mathrm{O_2}]k_{ox} + k_2 + k_{-2})\right) + \\ + [\mathrm{F^-}]K_{inh}\left(k_{-1}^f k_{-2} + k_{-2}^f k_{-1} + [\mathrm{O_2}]\left(k_{ox}^f k_{-1} + k_{ox}^f k_2 + k_{-1}^f k_{ox} + k_2^f k_{ox}\right) + k_1\left([\mathrm{O_2}]k_{ox}^f + k_2^f + k_{-2}^f\right) + k_1^f([\mathrm{O_2}]k_{ox} + k_2 + k_{-2})\right)\Big]}$$

(Supporting Eq. S31)

where:

$$k_1 = k_1^f = k_0 e^{-\alpha(E - E_{T1}^0)\frac{F}{RT}}$$ (Supporting Eq. S32)

$$k_{-1} = k_{-1}^f = k_0 e^{(1-\alpha)(E - E_{T1}^0)\frac{F}{RT}}$$ (Supporting Eq. S33)

$$\frac{k_d^f}{k_a^f} = K_{inh}$$ (Supporting Eq. S34)

Here k_0 is the heterogeneous ET rate constant; k_2 and k_{-2} are forward and backward internal electron transfer rate constants, respectively (from T1 to T2/T3 Cu cluster); k_2^f and k_{-2}^f are forward and backward internal electron transfer rate constants with bound fluoride ion, respectively; k_{ox} and k_{ox}^f are bimolecular oxidation constants for native and inhibited enzyme, respectively; α is the charge transfer coefficient from Butler–Volmer formulation; and E_{T1}^0 is the redox potential of T1 Cu site, respectively. This mathematical description was applied to averaged forward and backward scan sides of CVs presented in Figure S2 A, with background currents removed; modelling results are presented in Table S5. In measurements illustrated by Figure S2 A, AuNP/MBA/LAC electrode was prepared by a procedure in which 5 µl of concentrated LAC solution (3.10 mg mL^{-1}) was dispensed on the tip of a AuNP/4-

MBA-covered electrode (*vide supra*). Unlike in the case of original LAC adsorption method, it was difficult to reliably establish enzyme concentration by the decrease of activity in concentrated adsorption solution, because: i) enzyme activity compared to control solutions changed by less than 5 %; ii) evaporation of the enzyme solution drop was unpredictable; iii) unbound 4-MBA might have influenced enzymatic activity. Therefore, the modelling was performed by using fixed k_{ox} and k_{ox}^{f} values taken from previous modelling results described by Eq. S15-22 and presented in Table S4, E_{T1}^{0} = 0.683 V, as determined by spectroelectrochemical experiments, and Γ^{Tot} as a variable. Surface plots generated by using calculated results and plotted over experimental data are presented in Figure S3. Data fitting was performed employing Wolfram Mathematica 9 software from Wolfram Research (Champaign, IL, USA). All the biocathodic curves at different NaF concentrations were included into a single global analysis model.

Surface enhanced Raman spectroscopy (SERS) measurements. SERS experiments were performed as described previously.[9] Briefly, spectra were recorded with Echelle spectrometer RamanFlex 400 from PerkinElmer (Shelton, CT, USA) equipped with thermoelectrically cooled (–50 °C) CCD camera and fibre-optic cable. A 785 nm laser beam was used as the excitation source. The laser power at the sample was restricted to 30 mW and the beam was focused to a 200 μm diameter spot on the electrode with a total integration time of 300 s. Measurements were carried out in a three-electrode moving cell, arranged with a flat circular gold electrode of 5 mm diameter, press-fitted into a Teflon rod, serving as working electrode, a platinum wire as counter electrode, and an Ag|AgCl|sat. KCl reference electrode. The working LAC-AuNP covered electrode was placed at a distance of 3 mm from the cell window. In order to reduce photo- and thermo-effects, the cell together with the electrodes was moved linearly with respect to the laser beam at a speed of about 15-25 mm s^{-1}.[10,11] The Raman frequencies were calibrated using the polystyrene standard spectrum (ASTM E 1840). Intensities were calibrated by using a NIST

intensity standard (SRM 2241). SERS experiments were conducted in 0.05 M K_2HPO_4 solution adjusted to pH 5.4 by KOH.

Determination of the redox potential of the T1 Cu site. The redox potential of the T1 site of *Didymocrea* sp. J6 LAC was determined by mediated spectroelectrochemical redox titration following the procedure reported previously.[12,13] The home-built spectroelectrochemical cell consisted of a 1 cm long gold capillary electrode with an inner diameter of 350 μm, serving both as the working electrode and as a cuvette with a total volume of 1 μl. The input and output optical fibres (FCB-UV 400/050-2 and FC-UV 200, respectively) were purchased from Ocean Optics (Dunedin, Florida, USA) and attached to the ends of the capillary. The system comprised a DH-2000 light source and an HR4000CG-UV-NIR spectrometer from Ocean Optics. The spectra were recorded with the Ocean Optics Spectra Suite software. The potential of the gold capillary electrode was controlled using a μAutolabIII/FRA2 potentiostat/galvanostat from Metrohm Autolab (Utrecht, The Netherlands). Two platinum wires served as counter electrodes, and a Ag|AgCl|3M KCl electrode, separated from the enzyme solution by two ceramic frits and a buffer solution salt bridge to exclude chloride, was used as the reference electrode. The working gold capillary electrode was cleaned for approximately 10 h in freshly prepared 3:1(v:v) 96% sulfuric acid: 30% hydrogen peroxide (piranha) solution. For the enhancement of electrochemical communication between electrode and enzyme molecules, the reduced forms of three redox mediators, $K_4[Fe(CN)_6]$, $K_4[W(CN)_8]$ and $K_4[Mo(CN)_8]$, were used. The final concentration of each compound in the cuvette was 1 mM, their redox potentials were 430, 520 and 780 mV *vs.* NHE.[14]

The titration procedure was started with addition of 108 μL of LAC solution (5.33 mg mL^{-1}) into the cell containing mediators dissolved in 10 mM potassium phosphate buffer solution, pH 7.0. Beginning at an electrode potential 500 mV *vs.* NHE, after reaching equilibrium (40 min from initial solution application), the potential was gradually increased by 50 mV steps. Between steps the setup was allowed to equilibrate for 5 min, after which the absorbance spectra were recorded. This procedure was repeated

until the potential had reached 1000 mV (oxidative scan) and changed back to 500 mV (reductive scan). The light passage was closed between spectra recordings in order to avoid unnecessary heating of LAC solution in the cell. The oxygen was assumed to be depleted in the solution – the presence of LAC and mediator in the cell, low electrode potential, and 40 min of equilibration time are good conditions for complete oxygen reduction to water.

To determine the redox potential of the T1 Cu site, the dependence of absorbance values at 600 nm (peak maximum) on the applied cell potential was taken into consideration. The data points were approximated with the Nernst equation:

$$E_i = E_{redox} + \frac{RT}{nF}\ln\left(\frac{rAbs_i}{1-rAbs_i}\right) \qquad \text{(Supporting Eq. S35)}$$

where E_i is the applied potential at the i^{th} step, E_{redox} is the redox potential of the T1 Cu site, n is the number of electrons involved in the redox process, and $rAbs_i$ is the relative absorption at the i^{th} step, calculated as:

$$rAbs_i = \frac{Abs_i - Abs_{min}}{Abs_{max} - Abs_{min}} \qquad \text{(Supporting Eq. S36)}$$

Here Abs_i is the absorbance value at the i^{th} step, while Abs_{max} and Abs_{min} are the maximum and minimum absorbance values, respectively.

Experimental results

Apparent bimolecular oxygen electroreduction constants. The calculated apparent bimolecular O_2 reduction constants, k_{ox} ((0.71–4.17) × 10^4 M^{-1} s^{-1}), are lower for *Didymocrea sp.* J6 LAC compared to other MCOs (*cf. ca.* 10^4 M^{-1} s^{-1} *vs.* ≥ 10^6 M^{-1} s^{-1}). However, the k_{ox} value in a phosphate buffer, pH 4.0, without sodium sulphate, was measured to be as high as 10^6 M^{-1} s^{-1}, which means that the calculated apparent O_2 reduction rate was lowered due to the presence of sulphate anions in WBS. However, lowered k_{ox} allowed us to perform proper bioelectrochemical investigations without the drawback of O_2 mass-transfer limitations.

Table S1. Typical dependence of LAC amount and maximum bioelectroreduction current on working electrode potential used during electrostatic adsorption of LAC on AuNP/LAC electrodes.

E_{ads}, mV	ΔA, %	Γ, pmol cm^{-2}	j, μA cm^{-2}	k_{red}, s^{-1}
200	20.4	329	110	3.47
400	18.6	301	180	6.20
600	19.2	310	232	7.76
800	13.6	220	493	23.2
1000	9.68	157	34	2.24

Notes: E_{ads} – electrode potential set during enzyme adsorption; ΔA - change of enzymatic activity in adsorption solution; Γ – amount of adsorbed LAC, normalized to the geometrical area of the electrode; j – observed maximum bioelectroreduction current density of the resulting system at 500 mV *vs.* NHE, normalized to the geometrical area of electrode; and k_{red} – observed enzymatic turnover rate, calculated as electrons per second per LAC molecule.

Table S2. Onset and half-wave potentials of CVs of oxygen bioelectroreduction on AuNP/LAC electrodes, presented in the left panel of Figure 2.

pH 4.0			**pH 5.5**			**pH 7.4**		
[F^-], mM	Onset potential, mV	Half-wave potential, mV	[F^-], mM	Onset potential, mV	Half-wave potential, mV	[F^-], mM	Onset potential, mV	Half-wave potential, mV
0	839	739	0	783	634	0	704	608
10	741	638	5	757	624	2.5	694	575
20	735	627	10	743	598	5	676	566
40	723	614	20	711	582	10	640	550
80	721	602	40	667	572	20	624	530
160	712	585	80	660	562	30	618	510

Table S3. Kinetic modelling results from measurements of ABTS and $K_4[Fe(CN)_6]$ oxidation by oxygen catalysed by *Didymocrea* sp. J6 LAC. Parameters k_{inact}, k_{ox}, and K_{inh} were obtained both from ABTS and $K_4[Fe(CN)_6]$ oxidation experiments, and the modelling results were within the margins of error presented in the table.

pH	k_{inact}, s^{-1}	K_{inh}, μM	k_{ox}, $M^{-1}s^{-1}$
4.0	0.71 ± 0.05	22.9 ± 0.2	$(4.17 \pm 0.06) \times 10^4$
5.5	0.037 ± 0.003	187 ± 3	$(2.31 \pm 0.02) \times 10^4$
7.4	0.12 ± 0.03	290 ± 20	$(7.14 \pm 0.07) \times 10^3$

Table S4. Calculated parameters of mathematical modelling of data presented in *Figure 2* using the scheme illustrated in *Figure 1B* and detailed in Eq. S15-S22.

Parameter	pH 4.0	pH 5.5	pH 7.4
k_0, s^{-1}	30 ± 1	3.4 ± 0.2	6.0 ± 0.4
k_{ox}, $M^{-1}s^{-1}$	(3.724 ± 0.006) × 10^4	(1.713 ± 0.009) × 10^4	(2.3 ± 0.2) × 10^4
$E^0_{T2/T3}$, mV	752 ± 1	674 ± 1	599 ± 3
α	0.31 ± 0.01	0.36 ± 0.01	0.13 ± 0.03
k_0^f, s^{-1}	7.0 ± 0.3	2.3 ± 1.5	0.36 ± 0.21*
k_{ox}^f, $M^{-1}s^{-1}$	(1.012 ± 0.007) × 10^4	(0.17 ± 0.03) × 10^4	(2.1 ± 168) × 10^{4} *
$E^{F0}_{T2/T3}$, mV	600 ± 1	570 ± 1	497 ± 94*
α^f	0.34 ± 0.03	0.21 ± 0.07	0.16 ± 0.02
K_{inh}, mM	5.63 ± 0.06	19.6 ± 0.7	6.9 ± 1.4

Note: Asterisk-marked values are difficult to establish due to low current density and narrow CV profiles of NaF-inhibited systems working at pH 7.4 (see Figure 2, bottom).

Table S5. Calculated parameters of mathematical modelling of data presented in Figure S2 A using the kinetic scheme illustrated in Figure 1A and detailed in Eq. S29-S34.

Parameter	Value
k_0, s^{-1}	18 ± 1
α	0.16 ± 0.02
Γ^{tot}, pmol cm^{-2}	45 ± 1
k_2, s^{-1}	(1.71 ± 0.07) × 10^3
k_{-2}, s^{-1}	0
k_2^f, s^{-1}	irrelevant (from 0 to ∞)
k_{-2}^f, s^{-1}	(1.0 ± 0.1) × 10^2
K_{inh}, mM	0.14 ± 0.01

Table S6. Comparison of approximate main parameters of LAC-based Au cathodes operating in acidic air-saturated electrolytes.

LAC	Maximal current density ($\mu A\ cm^{-2}$)	Onset *vs.* T1 site potentials (V *vs.* NHE)	Stability (% after 24 h)	Reference
Didymocrea sp.	900	0.82 *vs.* 0.68	20	*
Trametes hirsuta	8	0.80 *vs.* 0.82[i]	n.d.	19
Trametes hirsuta	40	0.85 *vs.* 0.82 [i]	70	20
Cerrena unicolor	3000 [iii]	0.80 *vs.* 0.81 [ii]	95	22
Trametes hirsuta	600	0.85 *vs.* 0.82 [i]	50	23

Note: *Present studies. (i) This value was taken from Ref. 18 taking into account the 0.02 V/pH-unit dependence of the redox potential of the T1 site of MCOs. (ii) This value was taken from Ref. 21 taking into account the 0.02 V/pH-unit dependence of the redox potential of the the T1 site of MCOs. (iii) In O_2-saturated electrolyte solution.

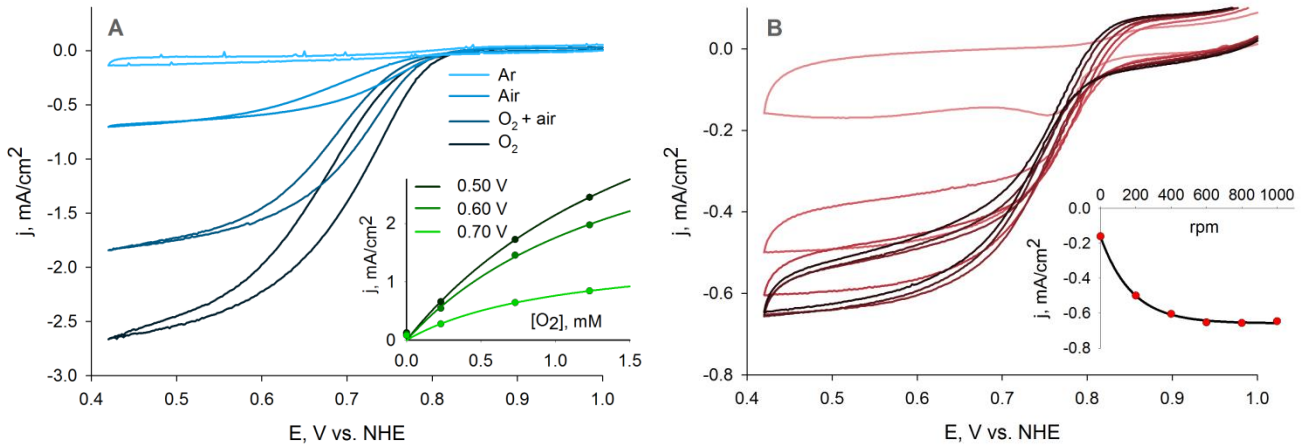

Figure S1. CVs of AuNP/LAC electrodes measured in WBS at pH 4.0, 23 °C, cathodic – anodic scan rate – 10 mV s^{-1}, at different O_2 concentrations and electrode rotation rates. (A) CVs of electrodes (1000 rpm) in WBS saturated with air, O_2, argon, and a 50/50% v/v mixture of WBS with air and O_2. *Inset:* O_2 concentration dependence of current densities at different potentials from CVs on; apparent Michaelis-Menten kinetic model is plotted over the data. (B) CVs of an electrode at different electrode rotation rates. *Inset:* dependence of current densities at 0.50 V on electrode rotation rate.

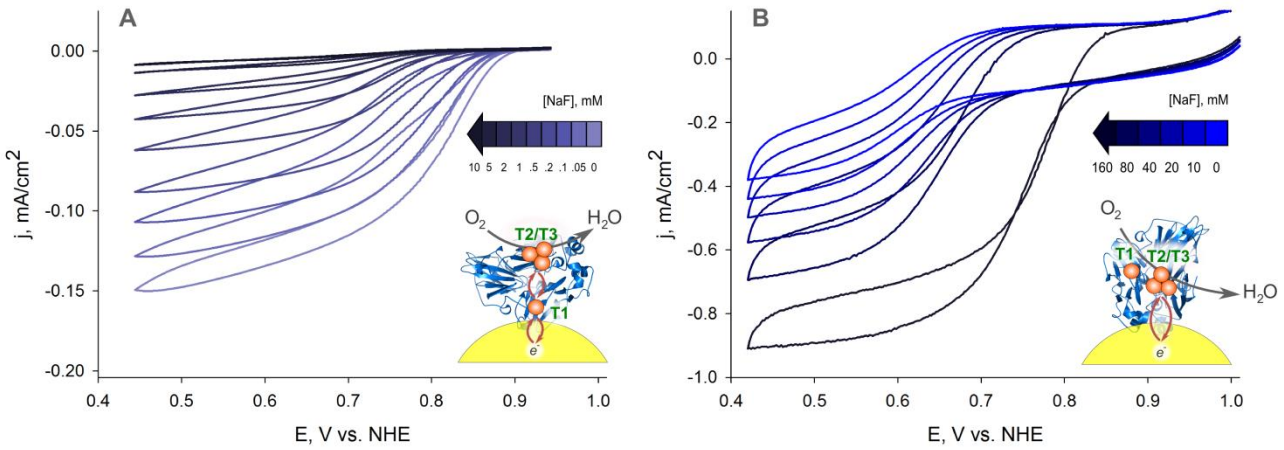

Figure S2. CVs of LAC-modified electrodes in WBS at pH 4.0 and different NaF concentrations, 23 °C, 1000 rpm, cathodic – anodic scan rate – 5 mV s^{-1}. The insets show suggested electron transfer pathways for each electrode. A) AuNP/MBA/LAC. B) AuNP/LAC.

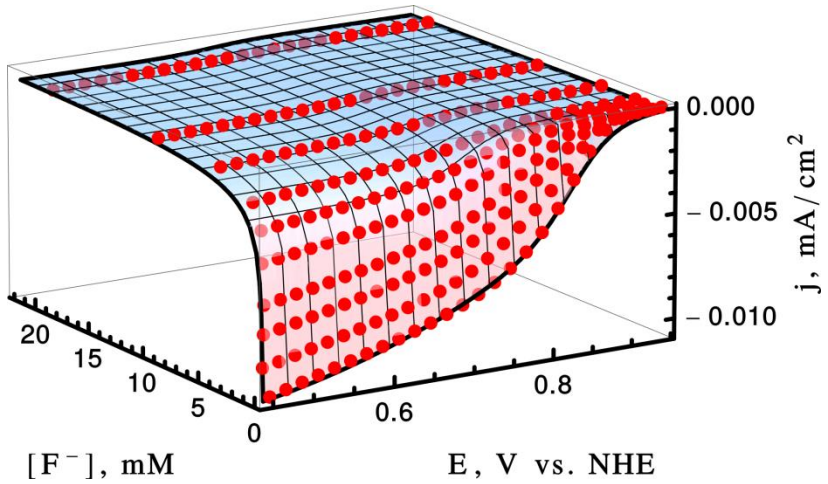

Figure S3. Surface plot (current density *vs.* electrode potential *vs*. NaF concentration) generated from the results of mathematical modelling (*vide supra*, Table S5) of background-current-subtracted averaged scan portions of CVs presented in Figure S2 A.

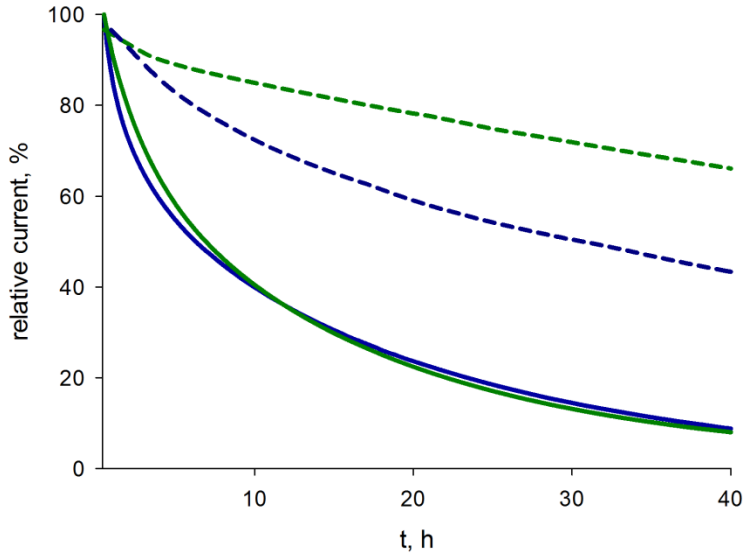

Figure S4. Change of relative current over time of continually operating electrodes (green curves – AuNP/LAC, blue – AuNP/MBA/LAC) at pH 4.0 (solid) and 7.4 (dashed). Conditions: WBS, 1000 rpm, 23 °C, working electrode potential set to 400 mV *vs.* NHE.

SERS measurements of LAC-AuNP-modified electrodes. In the fingerprint spectral region, the negative-going bands located at 1382, 1529, and 1633 cm^{-1} indicate an increase in intensity of these modes at more positive electrode potential, while the intensities of bands near 997, 1277, 1551, and 1677 cm^{-1} decrease (Figure S5, upper left panel). We assign the most intense band near 1382 cm^{-1} to stretching vibration of surface-bound carboxylate groups originating from the protein side chains. Previous SERS studies of peptides and amino acids have indicated enhancement and downshift (from 1403–1413 to 1383–1396 cm^{-1}) of symmetric stretching vibrations of the COO^- group, $\nu_s(COO)$, upon direct interaction with an electrode surface.[15,16] In the C–H spectral region, the broad positive-going band centred near 2830 cm^{-1} is visible in the difference spectrum (Figure S5, upper right panel). Previously, by analysis of SERS spectra of bifunctional alkanethiols adsorbed on Au and Ag electrodes, we have assigned a similar band to the "soft" C–H stretching mode of methylene groups directly interact-

ing with the metal surface.[17] The dependence of the intensity of ν_s(COO) and ν(C–H) soft modes on the electrode potential (Figure S5, bottom panel) indicates reorientation of adsorbed protein from a more extended, flat configuration at relatively negative electrode potentials (in which methylene groups directly contact the surface), to a more vertical orientation, in which interaction takes place mainly through the chemisorbed carboxylate groups of protein side chains (and in which protein methylene groups do not reach the metal surface).

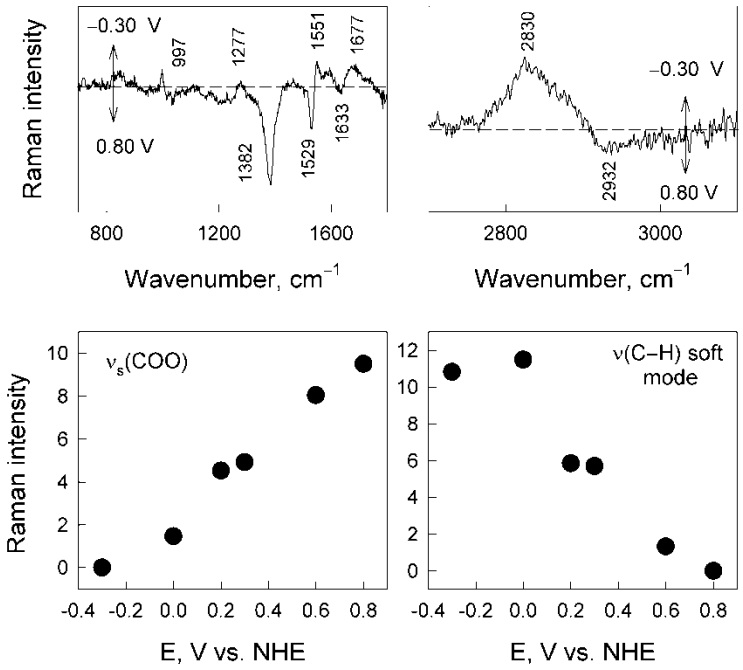

Figure S5. (Upper panels) Potential-difference SERS spectra of AuNP/LAC electrodes in the fingerprint (left side) and C–H stretching (right side) frequency regions. (Bottom panels) Electrode potential dependence of intensity of COO^- symmetric stretching mode near 1382 cm^{-1} from adsorbed carboxylate groups (left side) and intensity of C–H soft mode near 2830 cm^{-1} from methylene groups (right side). Note: the intensity of the soft band was obtained by subtraction of the spectrum at 0.80 V from that obtained at the given potential. The excitation wavelength was 785 nm (30 mW).

Discussion

Despite all experimental evidences for unique enzyme orientation presented above for the new AuNP/LAC electrodes, one can still try to explain the results of both electrodes using widely accepted enzyme electrokinetics developed by Armstrong with co-workers[24,25] based on the mechanism presented in Figure 1A. In WBS with acidic pH, the IET is fast and the T2/T3 Cu cluster is the control centre (*i.e.* the redox site up to which there is fast and reversible electron exchange with the electrode). Indeed, a 70 mV/pH-unit dependence of half-wave potentials has been obtained (Figure 2, top left; Table S2). At neutral or acidic pH in the presence of F^- the T1 site is the control centre since IET is slowed down, and again, lower half-wave potentials are registered along with only a 14 mV/pH-unit dependence (Figure 2, bottom left; Table S2). However, it is hard to believe that the bioelectrocatalytic response reflects the properties of T1 site in the case of AuNP/LAC electrodes because of too low values of registered half-wave potentials compared to the redox potential of the T1 site, *cf.* 627 and 716 mV (WBS, pH 4.0 in the presence of F^-), as well as 608 and 720 mV (WBS, pH 7.4 without F^-), especially taking into account fast heterogeneous ET in the LAC-AuNPs system.

Supporting references

1 L. Tetianec, A. Chaleckaja, R. Vidziunaite, J. Kulys, I. Bachmatova, L. Marcinkeviciene and R. Meskys, *J. Mol. Catal. B: Enzym.*, 2014, **101**, 28.

2 O. H. Lowry, N. J. Rosebrough, A. L. Farr and R. J. Randall, *J. Biol. Chem.*, 1951, **193**, 265.

3 E. I. Solomon, U. M. Sundaram and T. E. Machonkin, *Chem. Rev.*, 1996, **96**, 2563.

4 A. Laurynenas and J. Kulys, *Nonlinear Analysis: Modelling and Control*, 2014, **20**, 145.

5 J. Turkevich, P. C. Stevenson and J. Hillier, *Spec. Discuss. Faraday Soc.*, 1951, **11**, 55.

6 J. Kimling, M. Maier, B. Okenve, V. Kotaidis, H. Ballot and A. Plech, *J. Phys. Chem. B*, 2006, **110**, 15700.

7 W. Haiss, N. T. K. Thanh, J. Aveyard and D. G. Fernig, *Anal. Chem.*, 2007, **79**, 4215.

8 L. D. Burke and P. F. Nugent, *Gold Bull.*, 1997, **30**, 43.

9 M. Dagys, P. Lamberg, S. Shleev, G. Niaura, I. Bachmatova, L. Marcinkeviciene, R. Meskys, J. Kulys, T. Arnebrant and T. Ruzgas, *Electrochim. Acta*, 2014, **130**, 141.

10 G. Niaura, A. K. Gaigalas and V. L. Vilker, *J. Raman Spectrosc.*, 1997, **28**, 1009.

11 A. Bulovas, N. Dirvianskyte, Z. Talaikyte, G. Niaura, S. Valentukonyte, E. Butkus and V. Razumas, *J. Electroanal. Chem.*, 2006, **591**, 175.

12 A. Christenson, S. Shleev, N. Mano, A. Heller and L. Gorton, *Biochim. Biophys. Acta, Bioenerg.*, 2006, **1757**, 1634.

13 E. Osipov, K. Polyakov, R. Kittl, S. Shleev, P. Dorovatovsky, T. Tikhonova, S. Hann, R. Ludwig and V. Popov, *Acta Crystallogr., Sect. D: Biol. Crystallogr.*, 2014, **70**, 2913.

14 S. Tsujimura, A. Kuriyama, N. Fujieda, K. Kano and T. Ikeda, *Anal. Biochem.*, 2005, **337**, 325.

15 H. I. Lee, S. W. Suh and M. S. Kim, *J. Raman Spectrosc.*, 1988, **19**, 491.

16 J. S. Suh and M. Moskovits, *JACS*, 1986, **108**, 4711.

17 I. Razmute-Razme, Z. Kuodis, O. Eicher-Lorka and G. Niaura, *Phys. Chem. Chem. Phys.*, 2010, **12**, 4564.

18 S. Shleev, O. Morozova, O. Nikitina, E. Gorshina, T. Rusinova, V. Serezhenkov, D. Burbaev, I. Gazaryan, A. Yaropolov, *Biochimie* 2004, **86**, 693.

19 M. Dagys, K. Haberska, S. Shleev, T. Arnebrant, J. Kulys, T. Ruzgas, *Electrochem. Commun*., 2010, **12**, 933.

20 M. Pita, C. Gutierrez-Sanchez, D. Olea, M. Velez, C. Garcia-Diego, S. Shleev, V. M. Fernandez, A. L. De Lacey, *J. Phys. Chem. C*, 2011, **115**, 13420.

21 S. Shleev, M. Klis, Y. Wang, J. Rogalski, R. Bilewicz, L. Gorton, *Electroanalysis*, 2007, **19**, 1039

22 P. Olejnik, B. Palys, A. Kowalczyk and A. M. Nowicka, *J. Phys. Chem. C*, 2012, **116**, 25911.

23 C. Gutiérrez-Sánchez, M. Pita, C. Vaz-Domínguez, S. Shleev, A. L. De Lacey, *J. Am. Chem. Soc.*, 2012, **134**, 17212.

24 L. dos Santos, V. Climent, C. F. Blanford and F. A. Armstrong, *Phys. Chem. Chem. Phys.*, 2010, **12**, 13962.

25 C. Leger, S. J. Elliott, K. R. Hoke, L. J. C. Jeuken, A. K. Jones and F. A. Armstrong, *Biochemistry*, 2003, **42**, 8653.